STRONG GROUND MOTION SIMULATION OF THE 2019 JAVA, INDONESIA, EARTHQUAKE (*Mw* 6.9) USING EMPIRICAL GREEN'S FUNCTION METHOD

Ardian Yudhi OCTANTYO[1]
MEE19701

Supervisor : Hiroe MIYAKE[2]
Toshiaki YOKOI[3*]
Takumi HAYASHIDA[3**], **Saeko KITA**[3**],
Fumio TAKEDA[4**]

ABSTRACT

This study estimated strong motion generation area parameters and simulated the strong ground motion of the 2 August 2019 (*Mw* 6.9) intraslab earthquake and a hypothetical plate boundary earthquake (*Mw* 8.7) using the strong motion records of the 11 August 2019 (*Mw* 5.1) plate boundary earthquake with the empirical Green's function method. We first estimated the strong motion generation area that reproduced the strong ground motion during the *Mw* 6.9 intraslab earthquake, and conducted a rough estimation of the scaling parameters to see the impact of these parameters to the performance of the synthetic waveform reproduction. We also adjusted the stress drop ratio parameter (*C*) for some station records, which is sensitive to waveform amplitude. We then modeled the strong motion generation area of the *Mw* 8.7 hypothetical plate boundary earthquake using the *Mw* 5.1 plate boundary earthquake and the *Mw* 6.9 intraslab earthquake as the element events. The estimated peak ground acceleration values from the empirical Green's function simulation was compared with the conventional ground motion prediction equation. The comparison provided simulated acceleration level excited by a hypothetical *Mw* 8.7 that may occur in the future. The variability of simulated ground motion in terms of methods, source type as the element event, and rupture directivity effect was confirmed.

Keywords: Simulation, Strong Ground Motion, Peak Ground Acceleration, Ground Motion Prediction Equation, Empirical Green's Function Method.

1. INTRODUCTION

The Indonesia archipelago is one of the regions with the most concentrated seismic activity on the Earth. Five major tectonic plates interact within the Indonesia archipelago, in accordance with the MORVEL model (DeMets et al., 2010). One of the highest risk regions threaten by the seismic hazard is the Java island, the most populated island in Indonesia. The Java island region is overshadowed by the potencies for the next large earthquakes occurrence from the seismic activities of the off southern Java coast subduction zone. There is a possibility of seismic gap area lead by the indication of the interplate coupling activities (Hanifa et al., 2014) and lack of seismicity (PUSGEN, 2017) with the accumulated seismic moment equivalent to a *Mw* 8.7 earthquake. It is important to understand the strong ground motion characteristic triggered by a large earthquake, to anticipate recurrence of similar or larger earthquakes. But since the available historical information of the strong ground motion is limited, strong ground motion simulation may be helpful to fulfill the requirement of earthquake engineering application as well as the seismic hazard assessment.

This study applied the empirical Green's function method formulated by Irikura (1986) and Irikura and Kamae (1994) to perform the strong ground motion simulation for the most recent significant earthquake event of the 2 August 2019 Java intraslab earthquake (*Mw* 6.9) utilizing strong motion recordings of the 2019 Java plate boundary earthquake (*Mw* 5.1 and *Mw* 5.2) as the element events.

[1] Agency for Meteorology, Climatology and Geophysics, Republic of Indonesia.
[2] Associate Professor, Earthquake Research Institute, The University of Tokyo.
[3] International Institute of Seismology and Earthquake Engineering, Building Research Institute.
[4] National Graduate Institute for Policy Studies.
[*] Chief Examiner, [**] Examiner

Earthquake source parameter modeling is accomplished by following the recipe formulated by Miyake et al. (2003). We also tried to simulating strong ground motion for the maximum magnitude scenario earthquake in the same region (*Mw* 8.7) and performing the comparison of the simulated Peak Ground Acceleration (PGA) value obtained from the ground motion simulation with conventional ground motion prediction equations (GMPEs).

2. DATA

We selected the 2 August 2019 (*Mw* 6.9) intraslab earthquake as the target event for the strong ground motion simulation. However, this earthquake had a deficiency of aftershock and there is also no appropriate event having a similar characteristic with this earthquake in adjacent area. We decided to select plate boundary earthquakes occurred on 11 August 2019 with magnitudes *Mw* 5.1 and *Mw* 5.2, as the alternative element events to simulate the target earthquake, which were recorded at many strong motion observation stations. In present study we analyze the target event which were recorded at 47 INSMN stations located in the Sumatera and Java regions as well as the couple of earthquake events that act as the alternative Green's function element event.

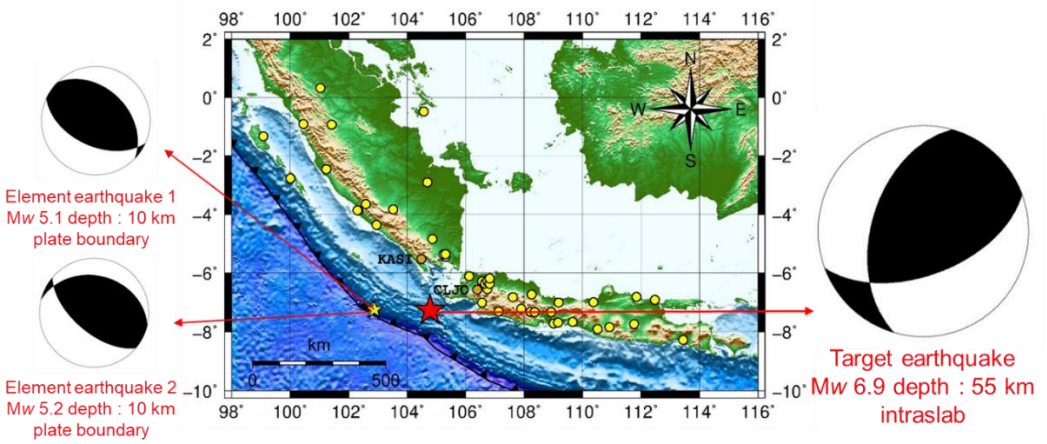

Figure 1. Hypocenters of the 2 August 2019 target earthquake along with alternative element earthquakes (parameter and focal mechanism by BMKG, 2019) and the 47 recorded strong motion stations (yellow dots).

3. THEORY AND METHODOLOGY

This study applied the empirical Green's function method by the formulation of Irikura (1986) and Irikura and Kamae (1994) to obtain well-performed strong ground motion simulation. This method utilized smaller event records to reproduce the ground motion simulation of a larger event, with the assumption that those small event records consolidate propagation paths and local site effects (Poiata and Miyake, 2017). The scaling relations between the target event and the element one in the empirical Green's function formulation are described into the ratio of fault dimensions (*N*) and stress drop (*C*) parameters, which is important to determined beforehand to obtain simulation of strong ground motion.

The parameters of *N* and *C* are determined by identifying the flat-level at the displacement and acceleration spectra amplitude of the two events. By the source spectral fitting, the estimation of the moment ratio of the target event to the element one event (M_0 / m_0), corner frequencies of the target event (f_{cm}) and the element one (f_{ca}) are provided. The relationships among the obtained parameters with the scaling parameters of *N* and *C* are described in Equations (1) and (2) as follows.

$$\frac{M_0}{m_0} = CN^3 \qquad (f \to 0)$$

$$\left(\frac{M_0}{m_0}\right)\left(\frac{f_{cm}}{f_{ca}}\right)^2 = CN \qquad (f \to \infty) \tag{1}$$

$$N = \frac{f_{ca}}{f_{cm}} \quad \text{and} \quad C = \left(\frac{M_0}{m_0}\right)\left(\frac{f_{cm}}{f_{ca}}\right)^3 \tag{2}$$

The target event waveform is reproduced by summing the waveforms of element events with adjustment for the difference in the slip velocity time function between the element event and the target event. The equation of summation is written as Equation (3),

$$U(t) = \sum_{i=1}^{N} \sum_{j=1}^{N} \frac{r}{r_{ij}} F(t) * (C \cdot u(t))$$

$$F(t) = \delta(t - t_j) + \frac{1}{n'\left(1-\frac{1}{e}\right)} \sum_{k=1}^{(N-1)n'} \left[\frac{1}{e^{\frac{(k-1)}{(N-1)n'}}} \delta \left\{ t - t_{ij} - \frac{(k-1)T}{(N-1)n'} \right\} \right]$$

$$t_{ij} = \frac{r_{ij} - r_o}{V_s} + \frac{\xi_{ij}}{V_r} \quad (3)$$

where U(t) represents the synthetic waveform of the target event, while u(t) the observed waveform of the element event, r the epicentral distance from each recording stations, V_s refers to S-wave velocity around source area and V_r refers to rupture velocity along the fault plane, while T is the rise time of the target event, *N* and *C* are the ratio of the fault dimension and stress drop of the target event to the element one, respectively, and F(t) is the filtering (adjustment) function for the difference in the slip velocity time function.

4. RESULTS AND DISCUSSION

4.1. Source parameters estimation for the 2 August 2019 (*Mw* 6.9) earthquake

Waveform data of the target event, as well as the waveform data of the 11 August 2019 (*Mw* 5.1) earthquake and the 11 August 2019 (*Mw* 5.2) earthquake as the element events, from the CLJO and KASI stations, were used to estimate the scaling parameter of fault dimension ratio (*N*) and stress drop ratio (*C*). We conducted a rough estimation of the scaling parameters to see the impact of these parameter to the performance of the synthetic waveform reproduction. We found that the stress drop ratio (*C*) parameter is sensitive to the amplitude of the synthetic waveform estimation for this pair of earthquakes. We had to assign the stress drop ratio (*C*) parameter separately for KASI station located in the azimuth direction of 350° and other stations that located in the azimuth direction range of 41° – 91° so the simulation of the synthetic waveform can be well performed. Detailed adjusted scaling parameters value is summarized in Table 1.

Table 1. Scaling parameters of the 2/08/2019 (*Mw* 6.9) target event pairs with the 11/08/2019 (*Mw* 5.1) element event.

No.	scaling parameters	KASI	other stations
1	f_{cm}	0.3 Hz	0.3 Hz
2	f_{ca}	0.9 Hz	0.9 Hz
3	*N*	3	3
4	*C*	10	10
5	propagation path adjustment coefficient	1	3
6	best fit *C*	10	30

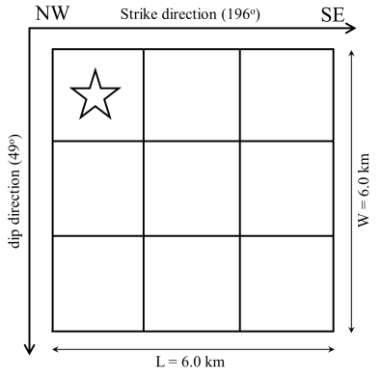

Figure 2. Strong motion generation area estimated to simulate the *Mw* 6.9 intraslab earthquake using the *Mw* 5.1 plate boundary earthquake.

Figure 2 shows the schematic model of the strong motion generation area for the target event. Sub fault dimension was set to be 2.0 km in length by 2.0 km in width, with the rise time of 0.2 second. Therefore, with the fault dimension ratio (*N*) equal to 3, the strong motion generation area dimension of the target event became 6.0 km in length by 6.0 km in width, with the rise time of 0.6 second and the initial rupture starting point at sub fault at the shallowest northern end of the strong motion generation area (1, 1).

Comparisons of the observed and synthetic waveforms for the KASI station and the CLJO station are provided in Figure 3. Here we found that through the adjustment application of the stress

drop ratio (*C*), adequate synthetized waveform of the estimated strong motion generation area can be achieved for acceleration, velocity and displacement pulses recorded at the two stations.

The adjustment for the parameter of stress drop ratio (*C*) was done to prevent too large miss estimation of the synthetic waveform reproduced from the element event waveform, since we used plate boundary earthquake records as the element to synthetize the waveform of the intraslab earthquake.

The difficulty to apply only one single source parameter as the input for the ground motion simulation performance can be influenced by the factors of lateral variations, attenuation structure, or other heterogeneity of subsurface structure along the propagation path, since we have significant different in depth, fault distance and azimuth degree between the pair of earthquakes. Another factor that might be involved is the differences in the source mechanism that are assumed to have homogeneous radiation pattern due to the scale of the magnitude.

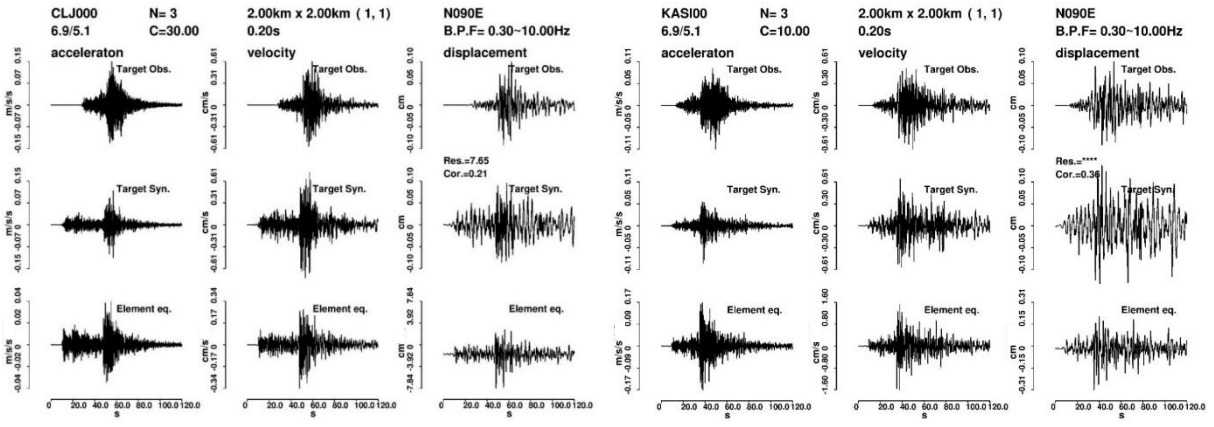

Figure 3. Ground motion simulation results of the CLJO and KASI stations (EW component).

4.2. Source parameters estimation for the *Mw* 8.7 hypothetical plate boundary earthquake

We tried several simulations scenario for the hypothetical plate boundary earthquake with *Mw* 8.7. First simulation utilizing the plate boundary earthquake *Mw* 5.1 as the element event, with the closest sub fault from the element event hypocenter as the rupture starting point (7,1). We also tried to assign the opposite direction rupture starting point (7,5) to see the sensitivity due to rupture propagation directivity. In the first step of the first simulation, we simulated a temporary earthquake event of *Mw* 6.9; we specified the *N* parameter of 10 and *C* parameter of 1. In the second step of the first simulation, we utilized the synthetic waveform from the temporary earthquake event, as the element input for the simulation of the target hypothetical plate boundary earthquake of *Mw* 8.7. We specified the final *N* parameter of 7 in length and 5 in width with *C* parameter of 1.

Determination of *N* parameter was done using scaling relations and other supporting information from previous studies. For *C* parameter we were consistently using the value of 1 by assuming same stress drop value between target and element events, and consider the simulations as the lower bound simulations. The *C* parameter controlled the amplitude of the simulated waveform, when we assigned larger *C* parameter, we will expect larger simulated peak ground acceleration.

Second simulation utilizing the intraplate earthquake *Mw* 6.9 as the element event, to find the possibility of using large intraslab earthquakes, that often occur inside the deeper part of the plate, to simulate the larger plate boundary earthquakes. Since we wanted to compare the results with the first simulation, we assigned one of the rupture starting points that is used in the first simulation, as the starting point of the second simulation. We also used the *N* and *C* parameters that already determined in the first simulation, without any adjustment. Radiation pattern correction was applied for the second simulation. The schematic illustration for the strong motion generation area of the *Mw* 8.7 hypothetical plate boundary earthquake are shown in Figures 4 and 5.

Simulated acceleration waveform and peak ground acceleration values of the hypothetical *Mw* 8.7 plate boundary earthquake for CLJO and KASI stations shows in Figure 6. The simulation result derived from the starting point (7,1) generally has larger PGA value compared to those derived from the starting point (7,5), that indicating the rupture directivity effect to the ground motions in each station.

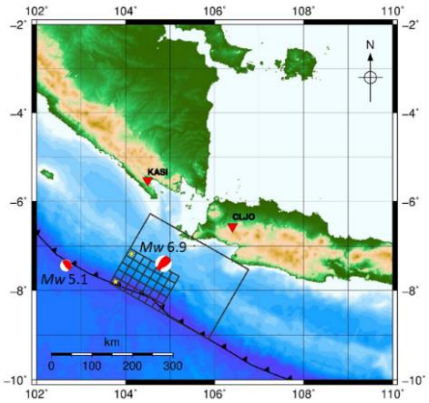

Figure 4. The *Mw* 8.7 hypothetical plate boundary earthquake simulation scheme.

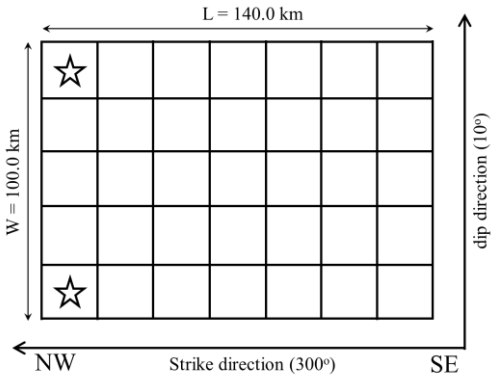

Figure 5. Strong motion generation area estimated to simulate the *Mw* 8.7 hypothetical plate boundary earthquake.

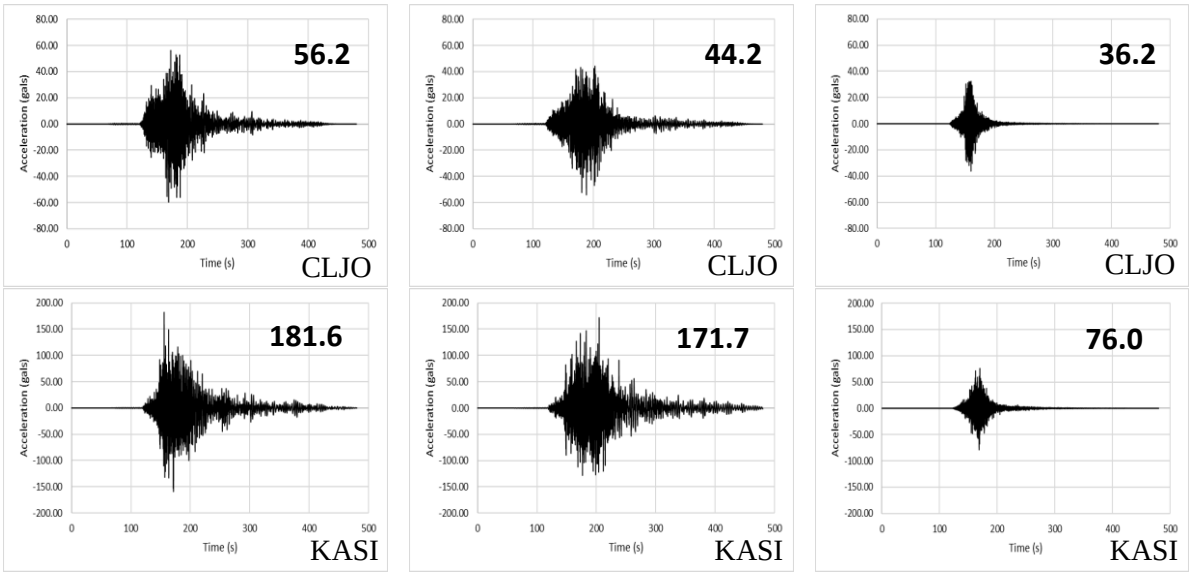

Figure 6. Simulated acceleration waveforms of the hypothetical *Mw* 8.7 plate boundary earthquake at CLJO and KASI stations (NS component). 1st column is the results for the 1st simulation with rupture starting point (7,1), 2nd column is for rupture starting point (7,5), and 3rd column is the results from the 2nd simulation with the rupture starting point (7,5).

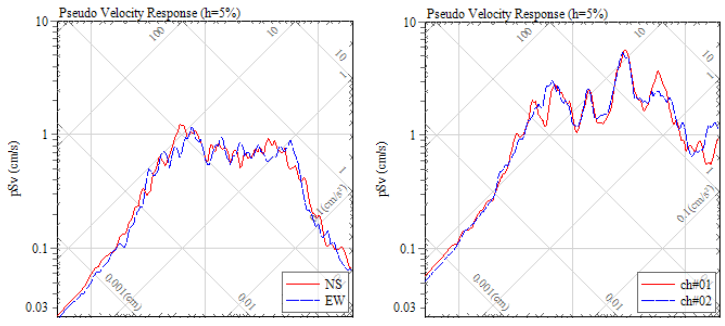

Figure 7. Comparison of the pseudo velocity response in Jakarta station between the *Mw* 6.9 intraslab earthquake (left figure) and the simulated *Mw* 8.7 hypothetical plate boundary earthquake (right figure).

4.3. The application of simulated ground motion: long-period ground motion in Jakarta

We applied the simulation of the *Mw* 8.7 hypothetical plate boundary earthquake using the *Mw* 6.9 intraslab earthquake as the element event in Jakarta. Here we would like to find the long-period ground motion contents and identify the characteristic behavior in the synthetic waveform resulting from simulation process. In Figure 7, we can notice from the flat level of the pseudo velocity response that the *Mw* 6.9 intraslab earthquake already contains long-period ground motion in Jakarta station ranging 0.5 - 7.0 seconds, and it was enhanced in the application result of the simulation for the *Mw* 8.7 plate boundary earthquake.

4.4. Comparison of the simulated PGA values from strong ground motion simulation and ground motion prediction equation (GMPE) for the *Mw* 8.7 hypothetical plate boundary earthquake

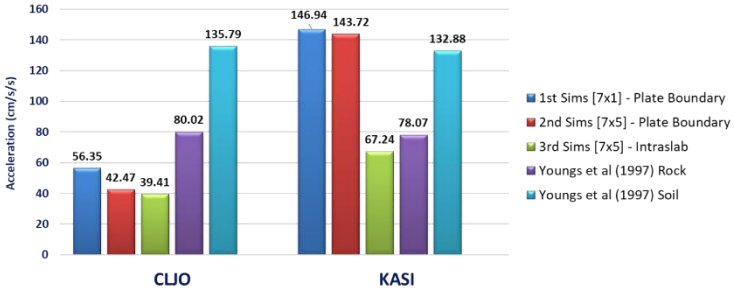

Figure 8. Comparison of the estimated PGA values obtained from the empirical Green's function simulations and GMPE by Youngs et al. (1997) for plate boundary source in rock and soil site conditions.

Comparisons between the results obtained from empirical Green's function simulation with ground motion prediction equation (GMPE) by Youngs et al. (1997) for the *Mw* 8.7 hypothetical plate boundary earthquake in CLJO and KASI stations, showed that GMPE calculation in CLJO station for rock condition was more comparable to the empirical Green's function simulation. While for KASI station, GMPE calculation for soil condition was more comparable to the empirical Green's function simulation. These differences were influenced by the local site condition in each station. Detailed estimated PGA values obtained from various methods are presented in Figure 8.

5. RECOMMENDATION

Hopefully in the future, the study of GMPE for Indonesia archipelago, can be well established along with the accumulation of strong ground motion records. So that, we can have better understanding on the strong motion attenuation relationship. Then, we can discuss the comparison with the empirical Green's function simulation from the point of view of PGA values.

We confirmed the variability of simulated ground motion in terms of various methodologies that we used to estimate the PGA values in this study as well as the variation of the source types that we used as the element event, and also the rupture directivity effect.

GMPE method and the empirical Green's function method often give different results, which bring us to a question "which one we should use as the appropriate estimation of PGA?". In this case, GMPE is more dependent, controlled by the constant, parameters and standard deviation that was already provided by the equation. On the other hand, empirical Green's function simulation is more independent; we can assign arbitrary parameters to obtain the simulation of the ground motion, and sometimes it becomes dangerous. So that, *N* and *C* parameters are crucial as the simulation control parameters. Supporting information regarding the parameters from previous study prior to the simulation will be helpful. Other idea is conducting trial simulations for all rupture starting points and calculate the average PGA value along with the standard deviation, to better fit the seismic hazard assessment.

ACKNOWLEDGEMENTS

I would like to acknowledge my sincere gratitude to my supervisor Dr. Hiroe Miyake and my advisor Dr. Toshiaki Yokoi for their perpetual guidance and support during this research work.

REFERENCES

DeMets, C., Gordon, R. G., and Argus D.F., 2010, Geophys. J. Int., 181, 1-80.

Hanifa, NR., Sagiya, T., Kimata, F., Efendi, J., Abidin, HZ., and Meilano, I., 2014, Earth Planet. Sci. Lett., 401, 159-171.

Irikura, K., 1986, Proceedings of the 7th Japan Earthquake Engineering Symposium, 151-156.

Irikura, K., and Kamae, K., 1994, Ann. Geofis., 37, 1721-1743.

Miyake, H., Iwata, T., and Irikura, K., 2003, Bull. Seis. Soc. Am., 93, 2531-2545.

National Center for Earthquake Studies of Indonesia (PUSGEN), 2017, Ministry of Public Works and Housing, Republic of Indonesia.

Poiata, N., and Miyake, H., 2017, Pure Appl. Geophys., 174, 3503-3519.

Youngs, R. R., Chiou S.-J., Silva W. J., and Humphrey J. R., 1997, Seismol. Res. Lett., 68, 58-73.